ChemElectroChem

Supporting Information

Gaining the Freedom of Scalable Gas Diffusion Electrodes for the CO_2 Reduction Reaction

Xin Wang[+], Chanikarn Tomon[+], Tim Bobrowski, Patrick Wilde, João R. C. Junqueira, Thomas Quast, Wenhui He, Nivedita Sikdar, Jonas Weidner, and Wolfgang Schuhmann*

Experimental Section:

Chemical and materials:

Cu nanoparticles (25 nm) were from Sigma Aldrich. PTFE dispersion with 210 nm PTFE particles (TF 5060GZ) was from 3M Dyneon. Isopropanol was from VWR Chemicals, and potassium hydroxide (KOH) was from Fisher Scientific. Super C65, TIMREX® SFG-44 and SFG-6 were from IMERYS GRAPHITE & CARBON. XPB-633 and XPB-538 were from Orion Engineered Carbons. The PEEK fabric mesh (PK-100/34) was purchased from Franz Eckert. The deionised water was from a Millpore purification system (18.2 MΩ). KOH was purified by a Chelex® resin column before use.

Characterisation:

Scanning electron micrographs (SEM) and FIB milling were performed using a Quanta 3D FEG ESEM (FEI) for SEM images and elemental mapping under the high vacuum mode with the voltage of 20.0 kV. The water contact angle was measured at ambient conditions with a custom-made water-contact angle goniometer using tri-distilled water. The gas products were analysed by multiple gas analyser #1 gas chromatograph (GC, SRI Instruments) with a flame ionisation detector methaniser (FID) and a thermal conductive detector (TCD). The TCD was used to detect H_2, and the FID was applied to detect CO, CH_4, C_2H_4, and C_2H_6. N_2 was the carrier gas, and the oven temperature was 90 °C. The liquid products were analysed by high-performance liquid chromatography (HPLC; Dionex ICS-5000) with a Diode Array Detector at 220 nm and a Refractive Index Detector (RefractoMax520). An ion-exclusion column from Bio-Rad (Aminex HPX-87H) was used as the column, and 4 mM H_2SO_4 was used as the eluent at an oven temperature of 70 °C.

Calculation of Faradaic Efficiency (FE %)[1]

Molar flow of gaseous products:

$$\dot{n}_i = x_i \frac{f}{V_m}, [\mathrm{mol \cdot s^{-1}}]$$

$\dot{n}_i$: molar flow of product *i*, mol·s^{-1}

x_i: concentration of the product *i*, vol%

f: CO_2/N_2 gas flow rate, L·s^{-1}

V_m: molar volume of an Ideal Gas = 24.5 L·mol^{-1} (25 °C)

Partial current:

$$I_i = z_i \dot{n}_i F, \ [\mathrm{A}]$$

I_i: partial current product *i*, A

z_i: number of electrons

$\dot{n}$: molar flow, mol·s^{-1}

F: Faraday constant, 96485 C mol^{-1}

Faradaic Efficiency:

$$FE_i = \frac{I_i}{I_t} \times 100, \ [\%]$$

FE_i: Faradaic efficiency product *i*, %

I_i: Partial current product *i*, A

I_t: Total current, A

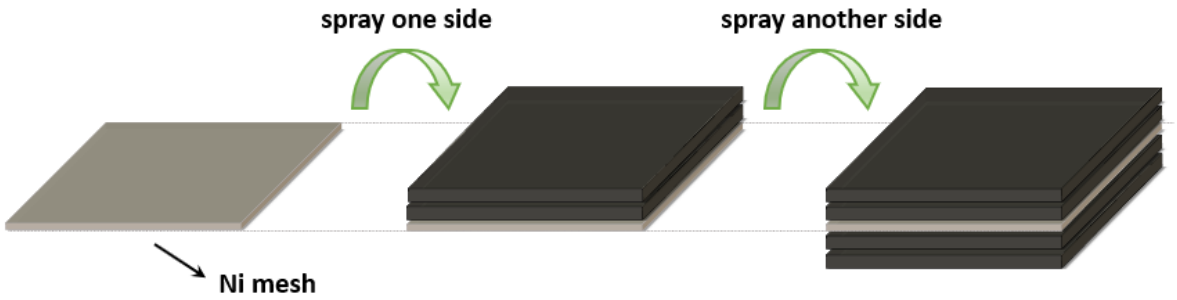

Figure S1. Scheme for the fabrication of a four-layers GDE with the same top and bottom layers.

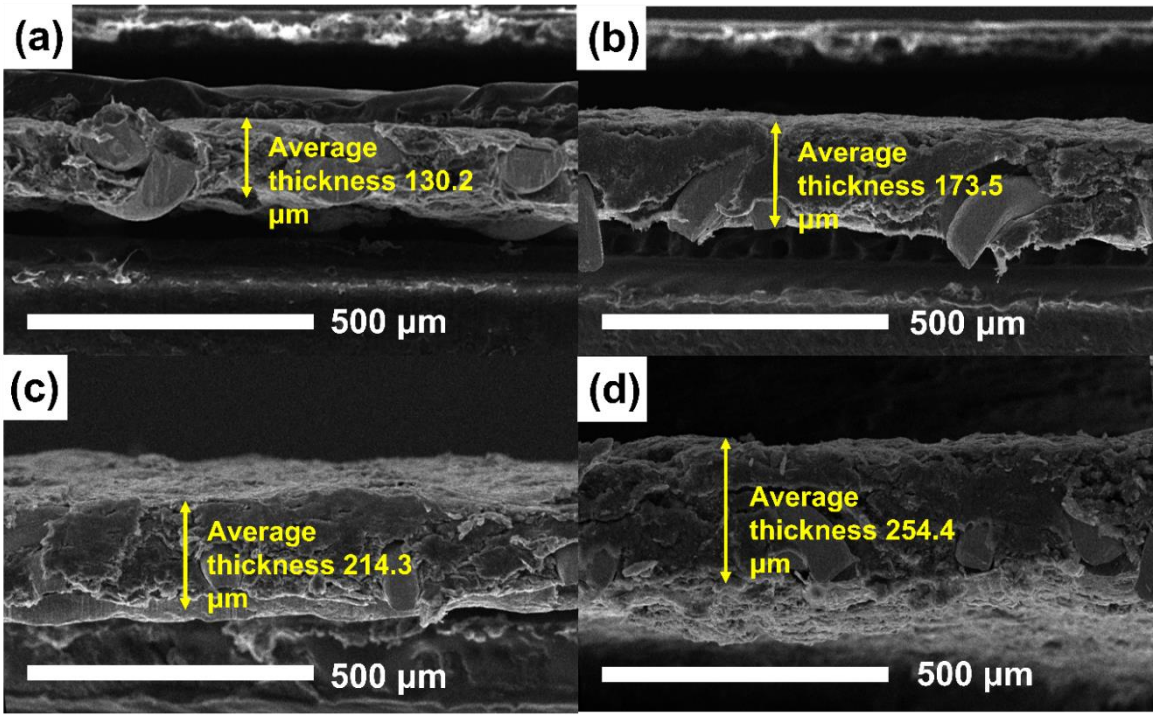

Figure S2. Cross-section SEM images of (a) 2-layer, (b) 3-layer, (c) 4-layer, and (d) 5-layer GDEs.

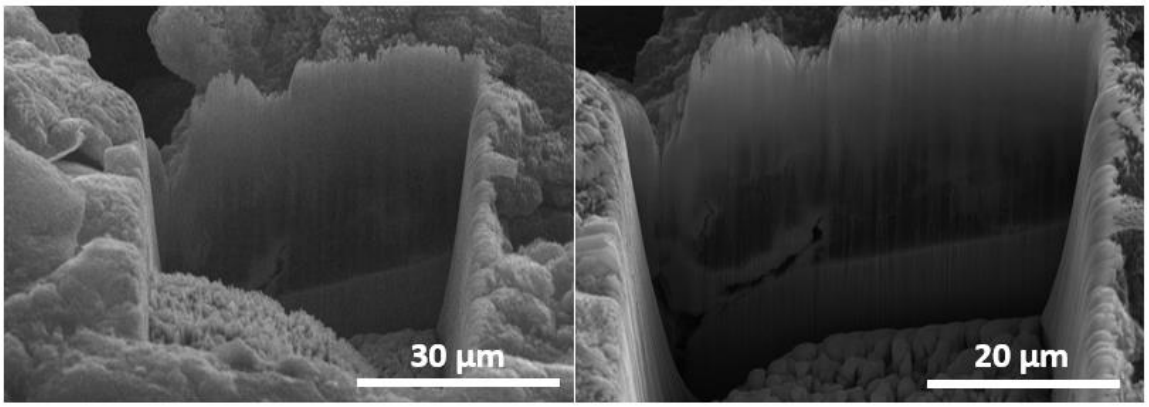

Figure S3. Cross-section SEM images after FIB-milling of a 4-layers GDE.

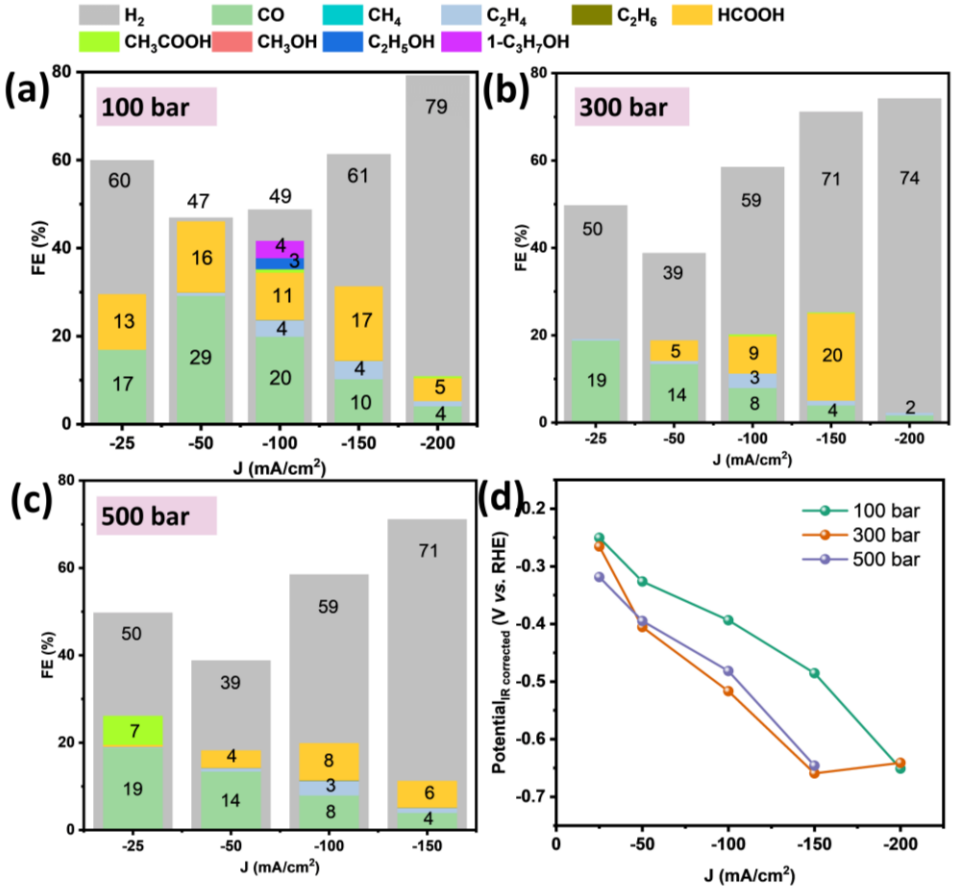

Figure S4. CO_2RR electrochemical performance of GDEs fabricated at different pressures during hot pressing. (a) 100 bar, (b) 300 bar, and (c) 500 bar. (d) Potentials of these three GDEs at the given current densities.

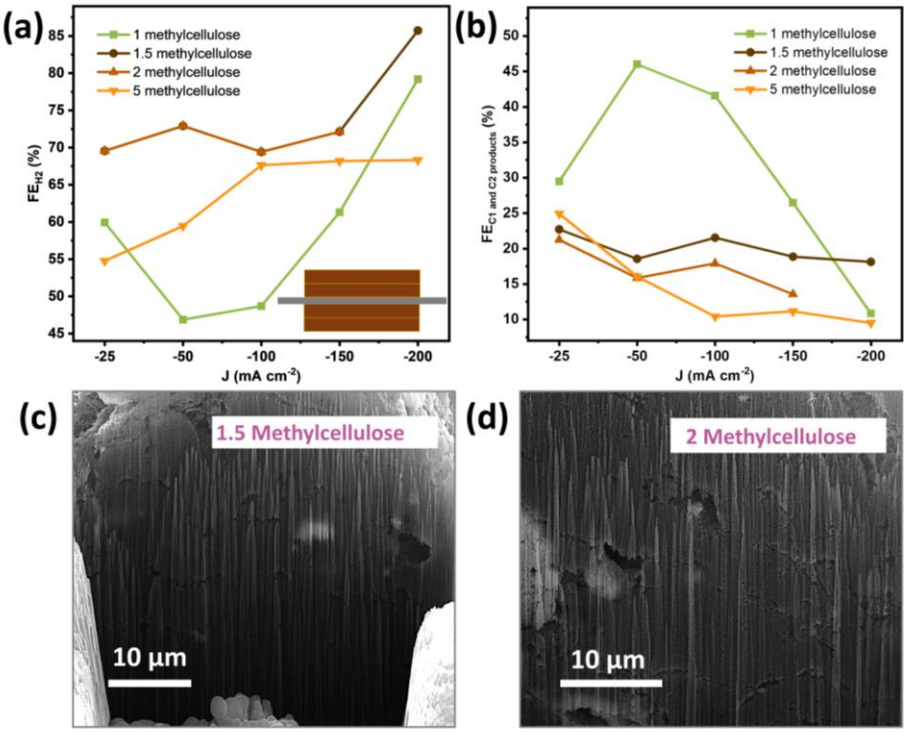

Figure S5. (a) H_2 production for different cellulose content. (b) CO2RR total C1 and C2 products for different cellulose amounts. Cross-section SEM images after FIB-milling of (c) 1.5 times the amount of cellulose, (d) 2 times the amount of cellulose.

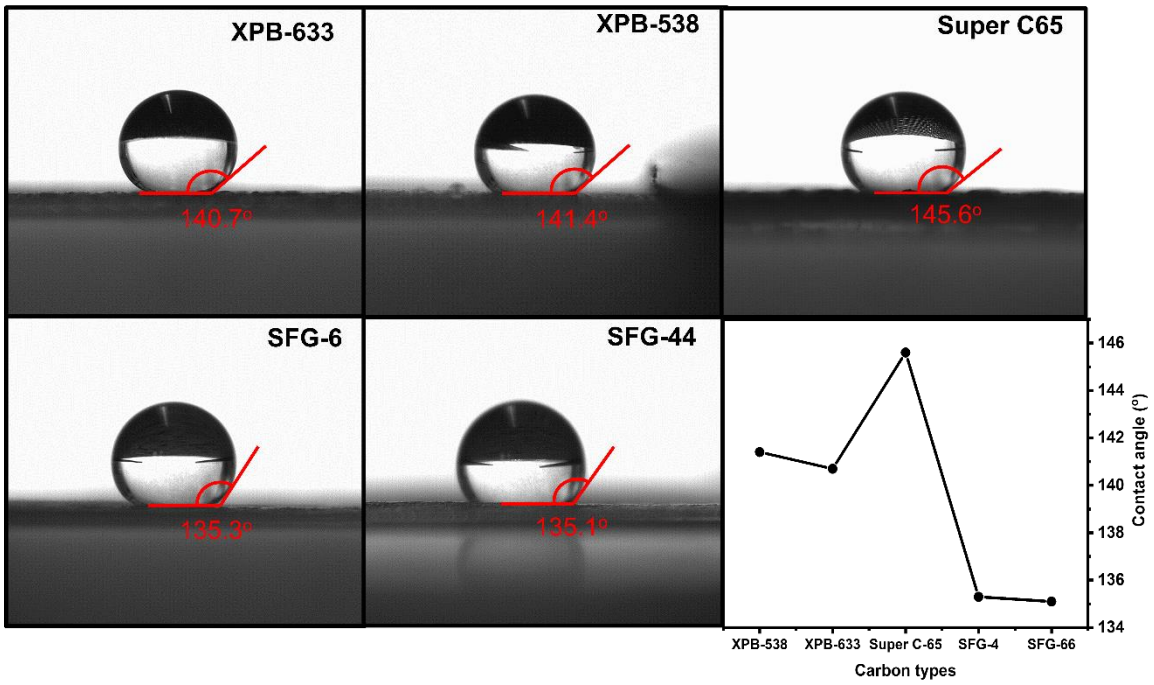

Figure S6. Contact angles of the GDEs using different carbon types, including XPB-633, XPB-538, Super C-65, SFG-6 and SFG-44.

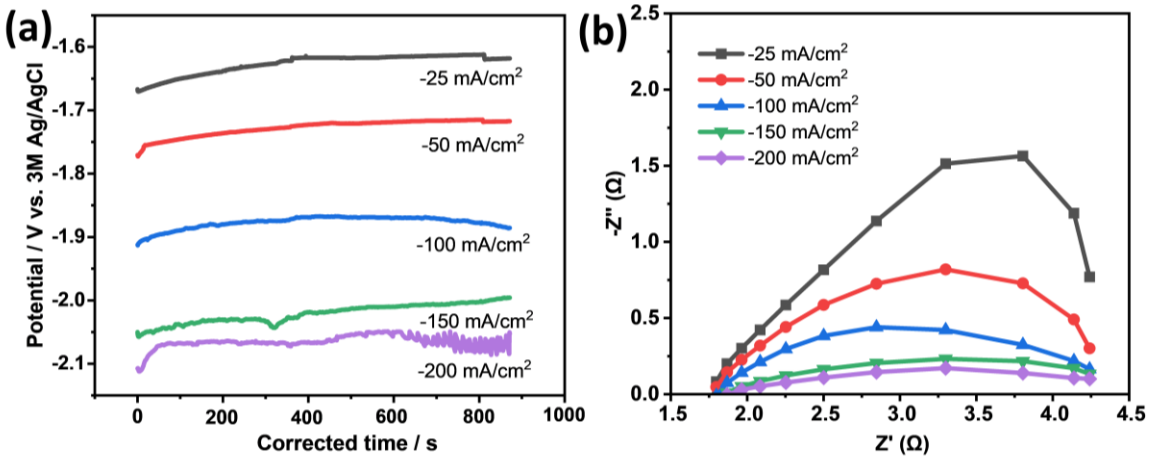

Figure S7. (a) The potential traces over time of the final GDE structure before iR compensation. (b) Corresponding galvanostatic impedance measurements of the final GDE structure at different current densities.

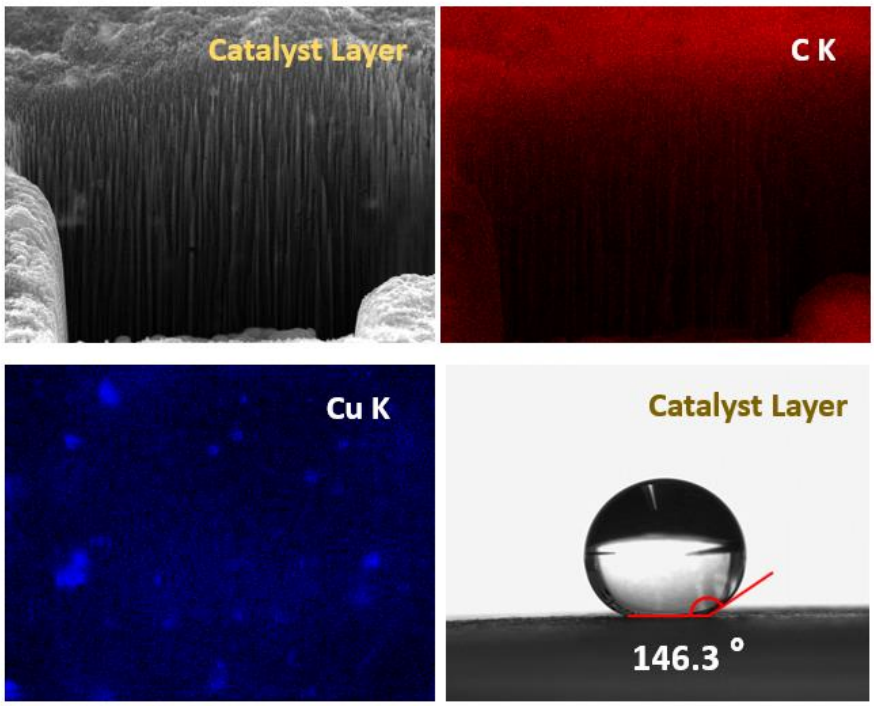

Figure S8. Cross-section elemental mapping images and water contact angle of the catalyst layer after FIB-milling.

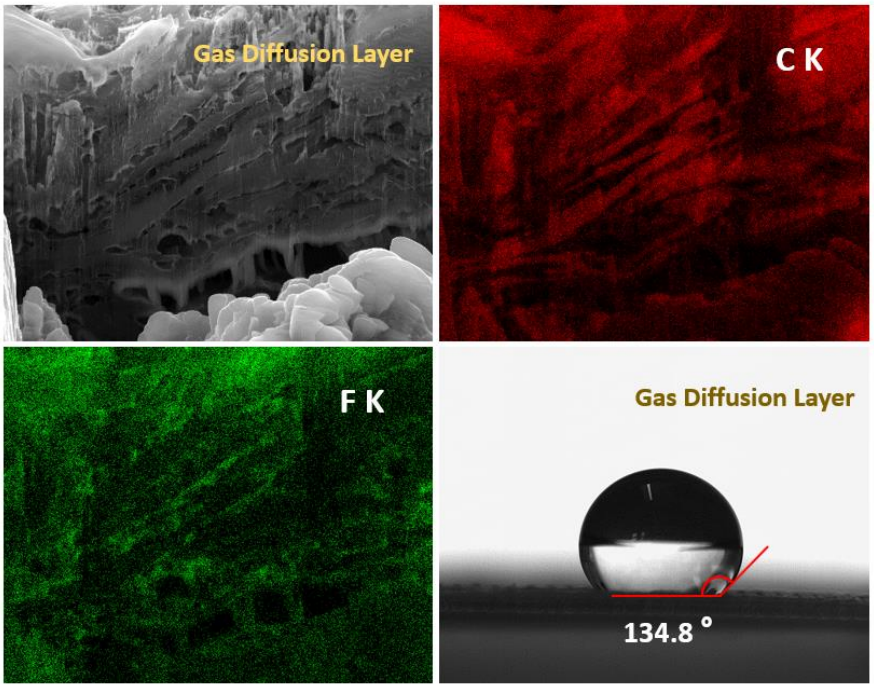

Figure S9. Cross-section elemental mapping images and water contact angle of the gas diffusion layer after FIB-milling.

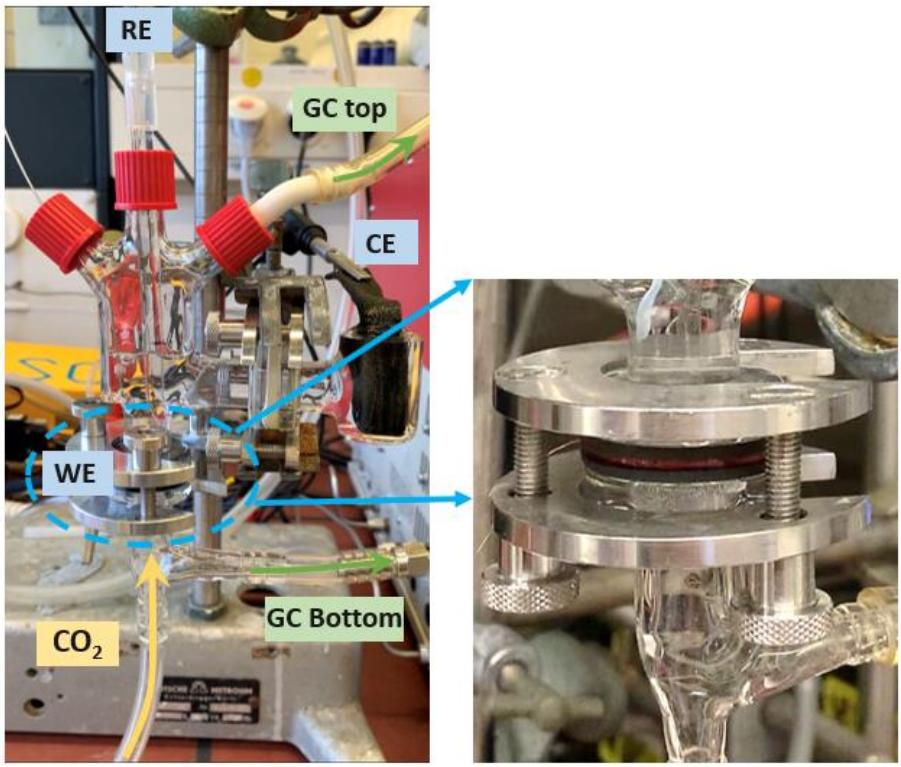

Figure S10. Configuration of the H-type cell and the connection to the GC.

Table S1. The properties of the studied carbon types [2]

Carbon	Structure	Particle size	Density	BET surface area	Resistance
SFG-44	synthetic graphite	< 44 µm	0.19 g/cm^3	5 m^2/g	12.32 Ω
SFG-6	synthetic graphite	< 10 µm	0.07 g/cm^3	17 m^2/g	12.98 Ω
XPB-538	amorphous	N/A	1.7 – 1.9 g/cm^3	1150 m^2/g	22.54 Ω
XPB-633	amorphous	10 – 200 nm	N/A	220 m^2/g	20.05 Ω
Super C-65	graphite nanoparticle	< 50 nm	1.60 g/cm^3	62 m^2/g	12.47 Ω

Note: The resistances of these 5 carbon materials were measured by ohmmeter.

References

[1] Z. P. Jovanov, J. Ferreira de Araujo, S. Li, P. Strasser, *J. Phys. Chem. C* **2019**, *123*, 2165.

[2] "Specialty carbon blacks" can be found under https://www.orioncarbons.com, 2019.